Kinetics of Sorption in Hygroscopic Hydrogels

NANO LETTERS

pubs.acs.org/NanoLett Letter

Kinetics of Sorption in Hygroscopic Hydrogels

Carlos D. Díaz-Marín,[§] Lenan Zhang,*[,§] Zhengmao Lu, Mohammed Alshrah, Jeffrey C. Grossman, and Evelyn N. Wang*

Cite This: https://doi.org/10.1021/acs.nanolett.1c04216 Read Online

ACCESS | Metrics & More | Article Recommendations | Supporting Information

ABSTRACT: Hygroscopic hydrogels hold significant promise for high-performance atmospheric water harvesting, passive cooling, and thermal management. However, a mechanistic understanding of the sorption kinetics of hygroscopic hydrogels remains elusive, impeding an optimized design and broad adoption. Here, we develop a generalized two-concentration model (TCM) to describe the sorption kinetics of hygroscopic hydrogels, where vapor transport in hydrogel micropores and liquid transport in polymer nanopores are coupled through the sorption at the interface. We show that the liquid transport due to the chemical potential gradient in the hydrogel plays an important role in the fast kinetics. The high water uptake is attributed to the expansion of hydrogel during liquid transport. Moreover, we identify key design parameters governing the kinetics, including the initial porosity, hydrogel thickness, and shear modulus. This work provides a generic framework of sorption kinetics, which bridges the knowledge gap between the fundamental transport and practical design of hygroscopic hydrogels.

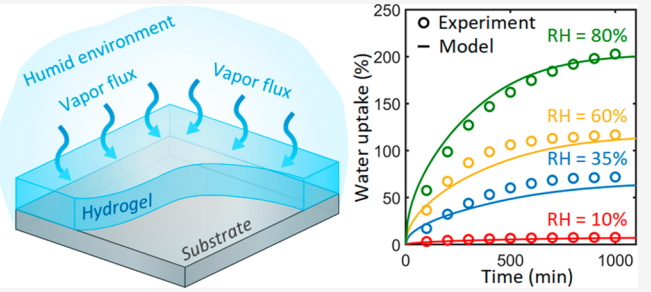

KEYWORDS: *Hydrogel, kinetics, sorption, water, vapor, diffusion*

Water sorption from the air is a ubiquitous phenomenon in nature and widely used in freshwater production,[1−5] passive thermal management,[6−10] and energy storage.[5,11−13] Hygroscopic hydrogels, which are capable of capturing and recovering water through sorption−desorption cycles, have become an emerging material for high-performance water sorption. These hydrogels typically exhibit fast sorption rates (fast kinetics), high sorbed water content (high water uptake), and large scalability.[14−17] In particular, tremendous experimental efforts have been carried out to optimize the chemical composition and material synthesis and therefore improve the water uptake and kinetics of hygroscopic hydrogels.[14,15,17−22] Yet, a mechanistic model to describe the underlying physics of sorption kinetics is lacking, which restricts the quantitative optimization toward the fundamental limit of the material.

Compared with typical sorption processes using solid-state sorbents such as silica,[23,24] zeolite,[25−27] and metal−organic framework,[1,28,29] the kinetics of hydrogel sorption is distinct due to the presence of gas, liquid, and polymer network. Therefore, conventional approaches by considering the vapor transport only are insufficient to describe the complex interactions during hydrogel sorption.[30,31] Figure 1a shows a schematic of the sorption process where a thin hydrogel layer is placed into a humid environment. By adding sorbents such as salts,[15,18] metal−organic frameworks,[17] or hygroscopic polymers[14] into the hydrogel, it becomes hygroscopic (Figure 1b−d). In general, three processes occur simultaneously inside the hydrogel: vapor transport, sorption, and liquid transport (Figure 1b−d). Vapor transport through the interconnected gaseous micropores relies on diffusion due to the presence of a vapor pressure difference (ΔP_v, Figure 1b,c). Sorption occurs on the liquid−gas interface of the micropores (Figure 1b,c). Meanwhile, liquid is transported through the nanopores of the polymer network (Figure 1b), driven by the water chemical potential difference ($\Delta\mu_l$) between the wet and dry regions of the polymer network (Figure 1d).[32] The redistribution of water leads to the structural change of micropores and polymer networks (Figure 1e−g) and further induces a volumetric expansion of the hydrogel due to the poroelastic effect.[8,33,34] This effect, in particular, is unique to hydrogels compared to other commonly used sorbent systems with rigid materials.[1,3]

In this work, we develop a generalized two-concentration model (TCM) for the kinetics of sorption in hygroscopic hydrogels. The simultaneous vapor and liquid transport during hydrogel sorption are described by two coupled diffusion equations, where the molar vapor concentration in the air C and the molar water concentration in the hydrogel relative to

Received: November 1, 2021
Revised: January 12, 2022

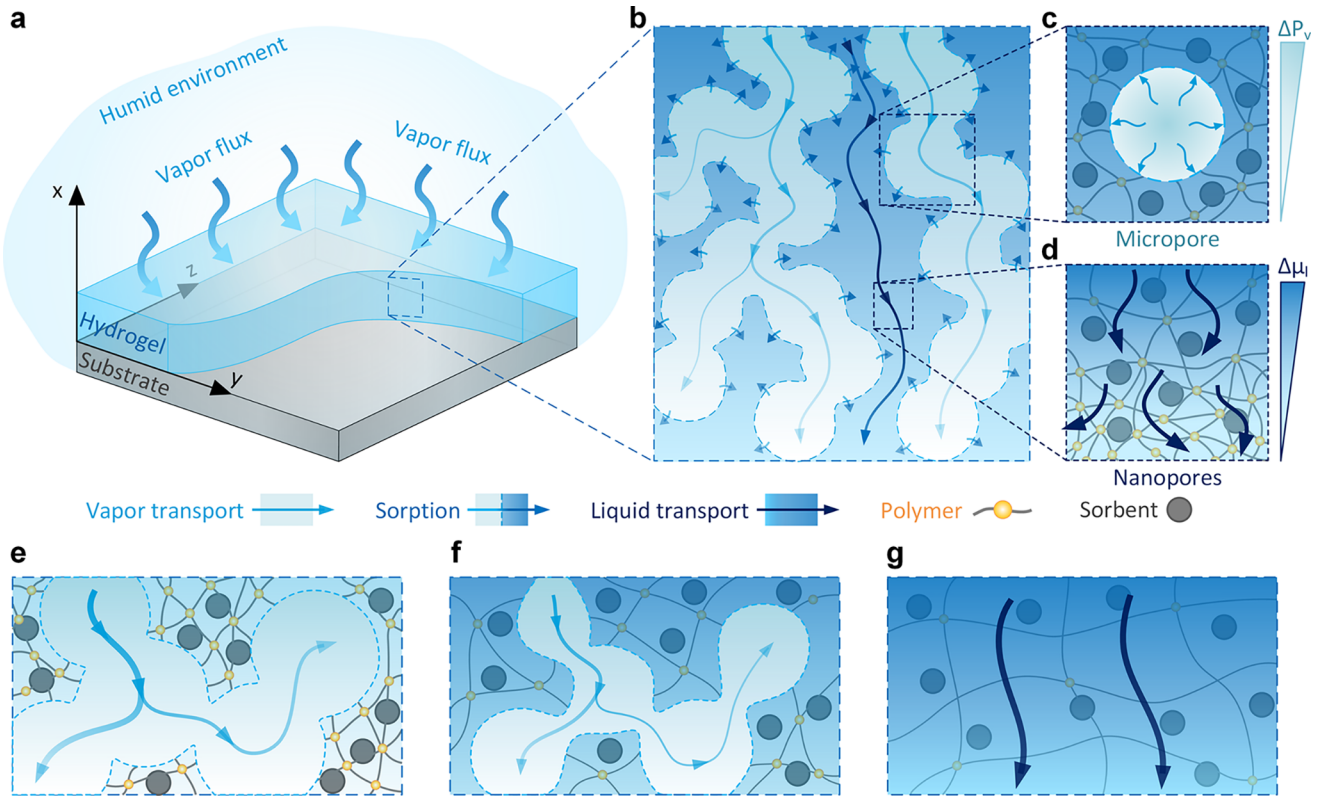

Figure 1. Sorption of hygroscopic hydrogel. (a) Schematic of the sorption of a thin hydrogel layer in a humid environment. (b) Complex transport across the hydrogel during the sorption process. Light blue arrow: vapor transport through the micropores (light blue region). Dark blue arrow: liquid transport through the nanopores of the polymer network (dark blue region). Blue dashed line: sorption at the liquid−gas interface. (c) Vapor transport in a single micropore. Vapor diffuses from the center to the wall of the micropore due to the reduced vapor pressure at the liquid−gas interface caused by the added sorbents. (d) Liquid transport through the nanopores of the polymer network. Liquid transport is driven by the gradient of water chemical potential, leading to the volumetric expansion of the polymer network. (e) Schematic of the hydrogel microstructure at the initial stage of sorption. Gaseous micropores occupy most of the volume and the polymer network contains a small amount of water. Vapor transport through the micropores is significant (light blue arrow). (f) Schematic of the hydrogel microstructure at the intermediate stage of sorption. Micropores shrink due to the increased amount of water and the expansion of the polymer network. (g) Schematic of the hydrogel microstructure at the end of sorption. Micropores tend to disappear and the polymer network fully expands. Water concentration becomes uniform due to the liquid transport (dark blue arrow).

its dry volume n are governed by (see Supporting Information S1 and S2 for details of the derivation)

$$\frac{\partial(\phi_g C)}{\partial t} - \frac{\partial}{\partial x}\left(D_{eff}\frac{\partial C}{\partial x}\right) = NSD_v\left(\frac{a_{w,s}P_{sat}}{RT} - C\right) \quad (1)$$

$$(1-\phi_{g0})\frac{\partial n}{\partial t} - \frac{\partial}{\partial x}\left(D_l\frac{\partial n}{\partial x}\right) = -NSD_v\left(\frac{a_{w,s}P_{sat}}{RT} - C\right) \quad (2)$$

where ϕ_s, ϕ_l, and ϕ_g are the local volume fractions of solid (i.e., the polymer network), liquid, and gas phase, respectively. ϕ_{g0} is the initial volume fraction of the gas phase, x is the coordinate along the hydrogel thickness direction, and t is time. Note that eqs 1 and 2 consider one-dimensional transport, which is valid for the commonly used thin hydrogel layers.[8,14,15] D_{eff} and D_l are the effective diffusivities of vapor and liquid transport and are defined in detail in eqs 3 and 4. N is the micropore number density and S is the mass transport shape factor of a single micropore. R is the gas constant and T is the absolute temperature of hydrogel. P_{sat} is the standard state saturated vapor pressure of water at T. As an example, we used the salt embedded hydrogel, where the salt serves as the sorbent,[8,10,15,18] because the thermodynamics of salt sorption have been widely studied.[35−38] The presence of salt in the hydrogel reduces the vapor pressure of liquid water at the liquid−gas interface, which drives the vapor transport across the micropores (Figure 1b,c). Sorption relies on the vapor condensation at the liquid−gas interface inside the hydrogel (Figure 1c). The reduction of vapor pressure due to salt is quantified by the water activity $a_{w,s}$, which is defined as the ratio of the vapor pressure in salt solution to standard state saturated vapor pressure of water. $a_{w,s}$ is a function of the type of the salt, temperature, and the mass fraction of salt in water.[39]

Equation 1 describes the time-dependent vapor transport along the thickness direction of the hydrogel. The source term on the right-hand side of eq 1 represents the sorption in position x. In each single micropore, its wall contains the salt or salt solution, which is supported by the polymer network, whereas the micropore is filled by an air−vapor mixture (Figure 1c). The vapor pressure on the wall of the micropore is given by $a_{w,s}P_{sat}$. If the saturated vapor concentration on the wall of the micropore ($a_{w,s}P_{sat}/RT$) is smaller than the vapor concentration (C) inside this micropore, there is a net vapor flux from the center of the micropore to the wall, indicating that sorption occurs. The vapor transport resistance inside this micropore is quantified by the shape factor S. For a spherical micropore with radius r_p, $S = 8\pi r_p$ (see Supporting Information

https://doi.org/10.1021/acs.nanolett.1c04216
Nano Lett. XXXX, XXX, XXX−XXX

S5 for details of the derivation).[40] This microscopic description of the sorption in a single micropore is then interfaced with the macroscopic transport equation under an effective medium approach: a macroscopic position x consists of numerous micropores. A macroscopic quantity in position x (e.g., C and $a_{w,s}$) is an average value over all the corresponding micropores in the same macroscopic position. Therefore, the total contribution of micropore sorption is given by the product of the single micropore sorption and pore number density, as captured by the right-hand side of eq 1. The effective vapor diffusivity accounts for the additional resistance to vapor transport due to the porous structure, which is given by

$$D_{\text{eff}} = \frac{D_v \phi_g}{\tau_g} \tag{3}$$

where D_v is the bulk diffusivity of vapor in air and τ_g is the tortuosity of the micropores. Since the hydrogel is a random porous medium, we take $\tau_g = \phi_g^{-1/2}$.[41,42] Note that sorption through liquid-to-vapor phase change leads to the shrinkage of the pore size, decrease of the salt mass fraction, and change of porosities (Figure 1e−g). Therefore, r_p, ϕ_s, ϕ_l, ϕ_g, and, $a_{w,s}$ are all time- and space-dependent variables (see eqs S28, S18−S20, and Figure S2, respectively).

Equation 2 is coupled with eq 1 through the sorption term to conserve mass: the increase of liquid arises from the vapor condensation (Figure 1e−g). Because of the nonuniform distribution of water in the polymer network of hydrogel, there exists a gradient of water chemical potential (Figure 1d), driving the liquid transport and volumetric expansion of the polymer network.[32,34] The liquid diffusivity D_l, which accounts for liquid transport in the hydrogel, is derived from Biot's linear theory of poroelasticity by coupling the water chemical potential with the elastic energy of the hydrogel,[33,43,44]

$$D_l = \frac{2(1+\nu)G}{3(1-2\nu)\eta} k \tag{4}$$

where ν and G are the Poisson ratio and the shear modulus of the hydrogel, respectively. η is the dynamic viscosity of water. k is the permeability of the nanoporous polymer network, which is a function of ϕ_l. We adopted the common form of k[34,45]

$$k = \frac{k_0 \phi_l}{(1-\phi_l)^{1.5}} \tag{5}$$

where k_0 is a constant determined by fitting, which can also be connected to the geometric properties of the hydrogel nanopores.[33] As a result, D_l is also time- and space-dependent. Note that although we used the salt embedded hydrogel as an example, the TCM given by eqs 1 and 2 is generic. If other types of sorbents are used, the expression for the sorption term or the water activity on the right-hand side of eqs 1 and 2 needs to be changed based on the isotherm of the corresponding sorbents.[30,46]

To validate our approach, we modeled the sorption kinetics of a $CaCl_2$ embedded polyacrylamide-based (PAM) hydrogel, which has been previously studied in literature, and compared with the experimental data.[15] To make an accurate comparison, material properties of hydrogel used in the TCM are identical to the experimental conditions.[15] We established an empirical expression of water activity $a_{w,s}$, which allows us to capture the complex water capture of $CaCl_2$, from the formation of hydrates to its deliquescence in solution by fitting the experimental isotherm (see Supporting Information S4 for details).[47−50] This empirical expression, together with eqs 1−5, S14, S18−S21, S27, and S28, construct a closed-form equation system which can be numerically solved. Note that in these equations the water concentration n is defined based on the initial volume of hydrogel, whereas the volume fractions are defined based on the current volume of hydrogel. The vapor concentration C is defined based on the air volume (see Sections S1−S3 for details).

In the simulation, the hydrogel was maintained in an equilibrium condition with a relative humidity (RH) of 5%. After $t = 0$, the hydrogel was placed into an environment with an elevated RH (RH = 10%, 35%, 60%, and 80%) and the sorption process started. We defined water uptake as the ratio of the sorbed water mass to the initial mass of the hydrogel. Details of hydrogel material properties and boundary conditions are provided in Supporting Information S7 and S8. Figure 2 shows the water uptake as a function of time with

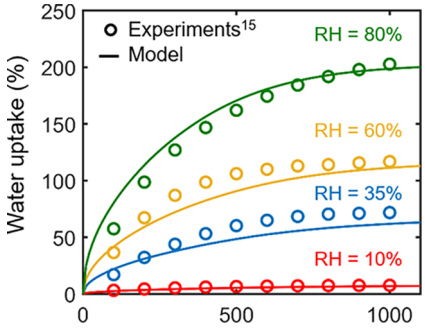

Figure 2. Hydrogel water uptake, defined as the mass of water captured from the ambient air divided by the initial hydrogel mass, as a function of time for different air relative humidities. Solid lines are computed based on our model by solving eqs 1 and 2. Markers correspond to experimental data from Li et al.[15] The model results agree well with the experimental results across all times and relative humidities corroborating the validity of our approach. The model results use a fitted permeability k that is consistent with the literature properties of the modeled PAM gel network.

four representative RH conditions. Good agreement between the experiment and simulation is shown. Note that although k_0 (6.74×10^{-18} m^2) was determined by fitting the experimental data, the same value of k_0 was used for all four RH conditions. More importantly, our fitted value of k_0 implies that the permeability of the polymer network reaches a value of about 1.5×10^{-17} m^2 (Figure S3), which agrees well with literature reported values of PAM hydrogels.[45,51] We further inversely estimated the nanopore diameter of about 28 nm based on the value of k_0, which lies in the literature reported range of PAM hydrogels[52,53] (see Supporting Information S9 for details). These agreements indicate that our TCM accurately captures the transport characteristics of the hydrogel and provides reasonable prediction for the sorption kinetics.

To understand the important role of liquid transport in the kinetics of hydrogel sorption, the simulation results were compared to a condition with vapor transport only by disabling liquid transport in eq 2 (*i.e.* $D_l = 0$). For the vapor transport only condition, we considered an identical $CaCl_2$ embedded PAM hydrogel with a theoretically minimum vapor transport resistance by setting its tortuosity $\tau_g = 1$ (eq 3). This condition is valid when the interconnected micropores are well-aligned

https://doi.org/10.1021/acs.nanolett.1c04216
Nano Lett. XXXX, XXX, XXX−XXX

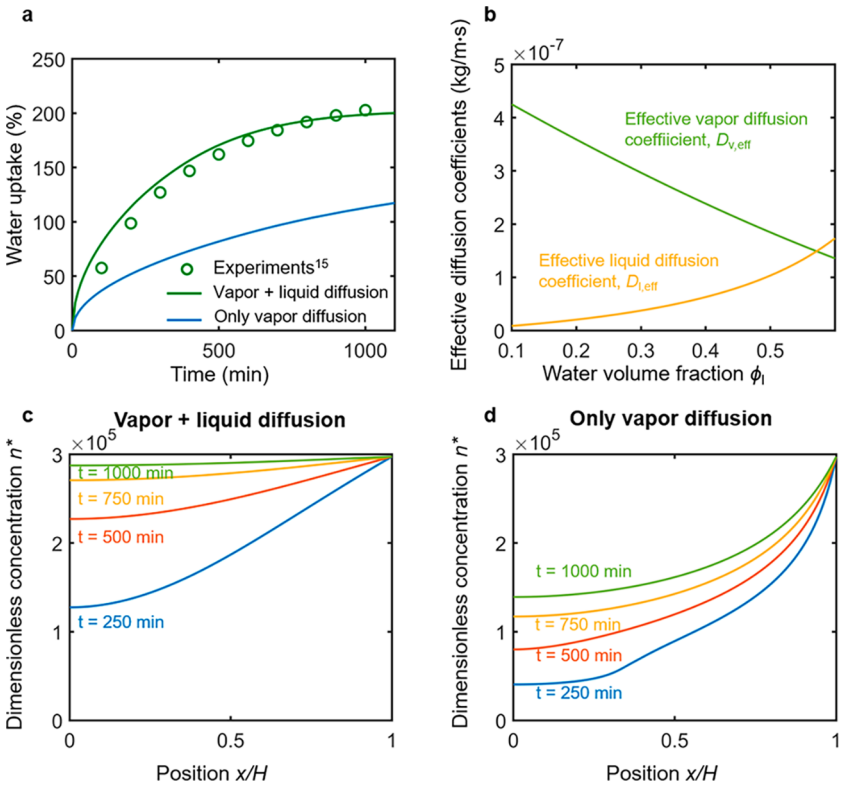

Figure 3. Impact of liquid transport in the sorption kinetics of hydrogel. (a) Uptake curves for a hydrogel with liquid and vapor diffusion and for a hydrogel with only vapor diffusion. A hydrogel without liquid diffusion has slower uptake than what has been reported experimentally. (b) Liquid effective diffusion coefficient, defined as $D_l \times \rho_l$, and vapor effective diffusion coefficient, defined as $D_{eff} \times \rho_v$, as a function of the liquid volume fraction ϕ_l. (c) Dimensionless water concentration $n^* = n/(P_{sat}/RT)$ inside the gel as a function of time for a hydrogel with both liquid and vapor diffusion. (d) Dimensionless water concentration $n^* = n/(P_{sat}/RT)$ inside the hydrogel as a function of time for a hydrogel with only vapor diffusion in the limit of unit tortuosity.

along the thickness direction and it, therefore, represents the fastest kinetics achievable with only vapor diffusion. Figure 3a shows the water uptake as a function of time with and without the contribution of liquid transport when RH = 80%. When only the vapor diffusion occurred, the hydrogel exhibited much slower sorption kinetics and cannot match the experimental data, even though the vapor transport resistance has already reached its theoretical minimum value. This comparison highlights the significant role of the liquid transport in the hydrogel sorption kinetics.

To elucidate the interplay between the liquid and vapor transport, we defined the effective diffusion coefficients of vapor transport and liquid transport as $D_{eff,v} = D_{eff} \times \rho_v$ and $D_{eff,l} = D_l \times \rho_l$, respectively, where ρ_v is the saturated vapor density and ρ_l is the water density. Figure 3b shows the effective diffusion coefficients as a function of liquid volume fraction ϕ_l. With the increase of ϕ_l, $D_{eff,v}$ decreases due to the reduction of the gas volume fraction (eq 3) whereas $D_{eff,l}$ increases because the hydrogel becomes more permeable to the liquid transport (eqs 4 and 5). We can therefore explain how the liquid transport enables the fast kinetics of hydrogel sorption. Figure 3c shows the dimensionless water concentration $n^* = n/(P_{sat}/RT)$) along the thickness direction where $x/H = 0$ represents the bottom of hydrogel and H is the initial thickness of the hydrogel. The top region close to $x/H = 1$ has higher water concentration and larger $D_{eff,l}$, driving the redistribution of water from the top to the bottom region. For this reason, n^* becomes more uniform with the increase of time (Figure 3c). However, when the liquid transport was disabled (Figure 3d), the accumulated water in the top region near $x/H = 1$ resulted in a significant resistance for the vapor transport (i.e., very low $D_{eff,v}$). Therefore, limited vapor flux reached the bottom region, leading to a nonuniform distribution of n^* along x as seen in Figure 3d and slower kinetics of sorption compared to the experimentally observed sorption (Figure 3a). Because of the lower water content, the concentration profile without liquid diffusion shows a transition between salt hydration and deliquescence, as seen by the inflection of the 250 min curve in Figure 3d.

To guide the design for practical applications, we performed a parametric study to identify the key parameters related to the kinetics of hydrogel sorption. For all of the simulations, we maintained the salt content as 3 g of salt per gram of hydrogel and only one parameter was varied in each time, relative to a controlled state with the same hydrogel properties as used in our validation (i.e., initial solid volume fraction $\phi_{s0} = 0.1$, micropore radius $r_p = 1$ μm, thickness of hydrogel $H = 5$ mm, shear modulus $G = 1000$ Pa). Figure 4a shows the impact of the initial solid volume fraction of hydrogel ϕ_{s0} on the kinetics of sorption. With the increase of ϕ_{s0}, the sorption kinetics first decrease and then increase, leading to a minimum value of kinetics. We quantified the kinetics of hydrogel sorption using an effective time scale τ, which is determined by fitting the water uptake to the following exponential relationship (see Supporting Information S10 for details of fitting)

$$\text{Uptake} = \text{Uptake}_{\infty}(1 - e^{-t/\tau}) \quad (6)$$

https://doi.org/10.1021/acs.nanolett.1c04216
Nano Lett. XXXX, XXX, XXX−XXX

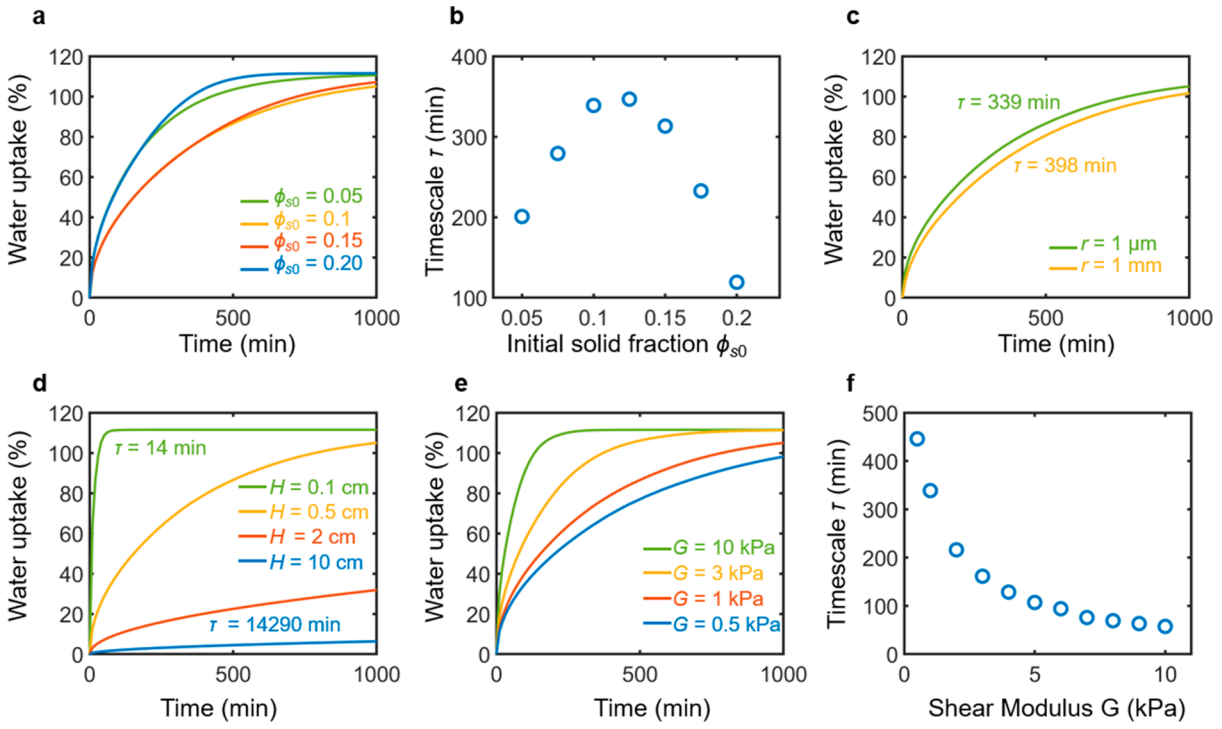

Figure 4. Impact of the different hydrogel properties in the kinetics of water uptake. (a) Water uptake curves as a function of time for different initial hydrogel solid volume fraction ϕ_{s0}. (b) Exponential decay time scale τ of the hydrogel sorption process, as defined by eq 6, as a function of the hydrogel initial solid fraction. (c) Water uptake curves as a function of time for two different hydrogel micropore radii of 1 μm and 1 mm. (d) Water uptake curves as a function of time for different hydrogel layer thicknesses H. (e) Water uptake curves as a function of time for different hydrogel shear modulus G. (f) Exponential decay time scale τ of the hydrogel sorption process as a function of the hydrogel shear modulus.

where Uptake_∞ is the equilibrium uptake determined by the water activity of salt solution and RH. The hydrogel approaches to its equilibrium state when $t \approx 3\tau$ (corresponding to more than 95% of the equilibrium uptake). Figure 4b shows the effective time scale τ as a function of the initial solid volume fraction ϕ_{s0}. The maximum value of τ = 347 min occurs at ϕ_{s0} = 0.125, corresponding to the slowest sorption kinetics. τ decreases from 347 to 119 min by increasing ϕ_{s0} to 0.2. This significant impact of the initial porosity on the kinetics can be explained by the interplay between the vapor and liquid transport. The amount of initial water contained in the hydrogel is determined by the amount of salt, which is proportional to the mass of the initially dried hydrogel. When the initial solid fraction is relatively high (e.g., ϕ_{s0} = 0.2), the amount of initial water in the polymer network is relatively high, leading to a rapid liquid transport (eq 4 and Figure 3b) and therefore accelerating the sorption kinetics. On the other hand, when the initial solid fraction becomes very low (e.g., ϕ_{s0} = 0.05), although the liquid transport is suppressed, vapor transport can be largely enhanced (eq 3 and Figure 3b) due to a higher gas volume and hence the sorption kinetics are faster.

Figure 4c shows that the micropore radius has negligible impact on the kinetics of hydrogel sorption. By increasing the micropore radius from 1 μm to 1 mm, there is only a slight increase of τ from 339 to 398 min. Although the sorption in each individual micropore highly depends on the micropore radius because the liquefaction rate in each micropore is related to its shape factor $S = 8\pi r_p$ (eqs 1 and 2), this resistance is several orders of magnitude smaller than the resistance due to vapor and liquid transport. On the other hand, reducing the layer thickness of hydrogel H can significantly accelerate the kinetics of sorption, because the resistance of both the vapor and liquid transport decreases with the H (Figure 4d). For example, the effective time scale decreased from 14 290 min to only 14 min by reducing H from 10 to 0.1 cm. τ shows a linear dependence with H as shown in Figure S6.

The coupling of the mechanical and transport properties in the hydrogel offers another opportunity space to engineer the sorption kinetics. Figure 4e shows water uptake as a function of time with four representative shear moduli G. The sorption kinetics increase with G due to the enhanced liquid transport (eq 4). Specifically, the effective time scale τ decreases from 446 to 57 min by increasing G from 0.5 to 10 kPa (Figure 4f). Although smaller τ can be achieved at higher G, the improvement of sorption kinetics by increasing G becomes less significant when G > 5 kPa.

The above parametric analysis provides quantitative design guidelines for hydrogel sorption. To achieve faster sorption kinetics, a hydrogel with high shear modulus and optimized initial solid fraction is desirable. In particular, given the wide-range of mechanical properties that can be achieved in hydrogels, with high-strength hydrogels exhibiting moduli exceeding the GPa range,[54] there is a large design space for the sorption kinetics of hygroscopic hydrogels by tailoring the liquid diffusion. A smaller effect in kinetics can also be achieved by tailoring the vapor diffusion through the hydrogel tortuosity (Figure S7).

Additionally, thinner hydrogel layers will also achieve faster sorption kinetics. Note that the thickness of hydrogel should be carefully chosen by considering the total water uptake. Although reducing the thickness can significantly decrease the effective time scale, the absolute amount of water uptake decreases simultaneously, which can be undesirable for practical implementations (see Figure S8). For example, in

https://doi.org/10.1021/acs.nanolett.1c04216
Nano Lett. XXXX, XXX, XXX−XXX

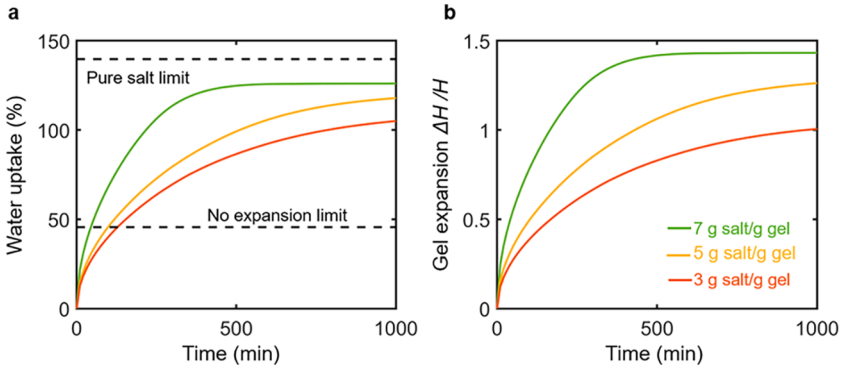

Figure 5. Impact of salt content in the sorption kinetics and water uptake of hydrogel. (a) Water uptake curves as a function time for different salt content of the hydrogel. Dashed lines correspond to the equilibrium water uptake for pure salt, which is the highest possible for a salt-embedded hydrogel without any additional sorption component, and to the no expansion limit, which represents the maximum water that can be accommodated inside the hydrogel if no volumetric expansion happened. (b) Increase in hydrogel thickness ΔH normalized by its initial thickness as a function of times for different salt loading.

the applications of water harvesting, energy storage, and thermal management, it is also important to match the kinetics of sorption with the operating cycles. If the effective time scale of sorption is much smaller than the duration of a cycle, the hydrogel reaches equilibrium much earlier before the cycle finishes, indicating a waste of operating time. However, if the effective time scale of sorption is much larger than the duration of a cycle, sorption does not finish in the end of this cycle, indicating a waste of material.

Finally, we show the impact of salt content on the equilibrium water uptake of hydrogel. Figure 5a shows the water uptake with different salt contents compared with the pure salt limit. The pure salt limit indicates the salt content reaching ∞ g/g hydrogel, that is, a condition without the polymer network. With the increase of salt content, the equilibrium water uptake approaches the pure salt limit gradually. Note that throughout this paper it was assumed that the equilibrium water uptake is determined by the salt content and its properties, as captured by eqs 1 and 2, which holds for hydrogels with large swelling ratios. In addition to the effect on equilibrium uptake, Figure 5a shows that the initial amount of salt can affect the kinetics of sorption. This can be explained by considering the variation in water content with salt content: for high salt content (7 g/g), the water content is high, leading to fast liquid diffusion (eqs 4 and 5).

In Figure 5a, the equilibrium water uptake was also compared with the no expansion limit. This limit is defined as the maximum amount of water that can be contained in a rigid hydrogel without volumetric expansion. Because of the volumetric expansion of hydrogel, more empty volume is created to contain the sorbed water. As a result, the equilibrium water uptake can be more than two times the no expansion limit and approaches the fundamental limit of salt sorption. As a comparison, for the conventional sorption based on solid foams, the theoretical maximum amount of water uptake is inherently limited by the volume of the foam. Therefore, the volumetric expansion highlights the advantage of hydrogel as a framework for sorption. Figure 5b shows the resulting increase of hydrogel thickness $\Delta H/H$ as a function of time. The final thickness can be more than two times of the initial thickness. More expansion was observed in the higher salt content conditions due to the higher equilibrium water uptake.

In summary, we developed a generalized model for the kinetics of sorption in hygroscopic hydrogels. Two governing equations were introduced to describe the coupled vapor and liquid transport during the sorption process. We validated our approach using experimental data. In addition to the vapor transport through micropores, we demonstrated the important role of liquid transport through the nanopores of the polymer network, which dominates the overall sorption kinetics in the regions with high water concentration. In addition, we showed that the volumetric expansion leads to the high water uptake, which approaches the thermodynamic limit of pure salt. Furthermore, we identified the key design parameters for the optimization of sorption kinetics due to the interplay of vapor and liquid transport. We showed that a thinner hydrogel layer with higher shear modulus and carefully chosen initial porosity is desirable for faster kinetics. This work elucidates the underlying physics of sorption kinetics in hygroscopic hydrogels. Our theory provides a general framework to understand the fundamental transport in hydrogel and guides the design of various sorption-based applications.

■ ASSOCIATED CONTENT

Supporting Information

The Supporting Information is available free of charge at https://pubs.acs.org/doi/10.1021/acs.nanolett.1c04216.

Derivation of vapor transport equation, derivation of liquid transport equation, equations for the volume fractions, activity function, shape factor for a pore, properties of hydrogel used on simulation, boundary conditions, calculation of permeability and pore size, time scales for uptake curves, thickness dependence of sorption kinetics, thickness dependence of total water captured (PDF)

■ AUTHOR INFORMATION

Corresponding Authors

Evelyn N. Wang − *Department of Mechanical Engineering, Massachusetts Institute of Technology, Cambridge, Massachusetts 02139, United States;* orcid.org/0000-0001-7045-1200; Email: enwang@mit.edu

Lenan Zhang − *Department of Mechanical Engineering, Massachusetts Institute of Technology, Cambridge,*

https://doi.org/10.1021/acs.nanolett.1c04216
Nano Lett. XXXX, XXX, XXX−XXX

Massachusetts 02139, United States; orcid.org/0000-0002-8740-2736; Email: lzhang2@mit.edu

Authors

Carlos D. Díaz-Marín − *Department of Mechanical Engineering, Massachusetts Institute of Technology, Cambridge, Massachusetts 02139, United States;* orcid.org/0000-0002-1890-4863

Zhengmao Lu − *Department of Materials Science and Engineering, Massachusetts Institute of Technology, Cambridge, Massachusetts 02139, United States;* orcid.org/0000-0002-5938-717X

Mohammed Alshrah − *Department of Mechanical Engineering, Massachusetts Institute of Technology, Cambridge, Massachusetts 02139, United States;* orcid.org/0000-0002-9796-9840

Jeffrey C. Grossman − *Department of Materials Science and Engineering, Massachusetts Institute of Technology, Cambridge, Massachusetts 02139, United States;* orcid.org/0000-0003-1281-2359

Complete contact information is available at: https://pubs.acs.org/10.1021/acs.nanolett.1c04216

Author Contributions

[§]C.D.D. and L.Z. contributed equally to this work.

Author Contributions

L.Z. and C.D.D. conceived the initial concept. L.Z., C.D.D., and Z.L. derived the governing equations. C.D.D. performed the numerical simulations. C.D.D., L.Z., Z.L., and M.A analyzed the results. C.D.D and L.Z. wrote the manuscript with input from all coauthors. E.N.W., L.Z., and J.C.G. supervised the project.

Notes

The authors declare no competing financial interest.

■ ACKNOWLEDGMENTS

C.D.D. gratefully acknowledges financial support from the Air Force Office of Scientific Research under Grant No. FA9550-19-1-0392 with Dr. Ali Sayir as program manager and a Professor Amar G. Bose Research Grant. L.Z. and E.N.W acknowledge support from the Singapore-MIT Alliance for Research and Technology (SMART) LEES Program. L.Z. gratefully acknowledges the MIT Martin Family Society of Fellows for Sustainability and Abdul Latif Jameel Water and Food Systems Lab (J-WAFS). M.A. acknowledges the financial support from the Natural Sciences and Engineering Research Council of Canada (NSERC).

■ REFERENCES

(1) Kim, H.; Yang, S.; Rao, S. R.; Narayanan, S.; Kapustin, E. A.; Furukawa, H.; Umans, A. S.; Yaghi, O. M.; Wang, E. N. Water Harvesting from Air with Metal-Organic Frameworks Powered by Natural Sunlight. *Science (80-.).* **2017**, *356* (6336), 430−434.

(2) Kim, H.; Rao, S. R.; Kapustin, E. A.; Zhao, L.; Yang, S.; Yaghi, O. M.; Wang, E. N. Adsorption-Based Atmospheric Water Harvesting Device for Arid Climates. *Nat. Commun. 2018 91* **2018**, *9* (1), 1−8.

(3) LaPotin, A.; Zhong, Y.; Zhang, L.; Zhao, L.; Leroy, A.; Kim, H.; Rao, S. R.; Wang, E. N. Dual-Stage Atmospheric Water Harvesting Device for Scalable Solar-Driven Water Production. *Joule* **2021**, *5* (1), 166−182.

(4) Hanikel, N.; Prévot, M. S.; Yaghi, O. M. MOF Water Harvesters. *Nat. Nanotechnol. 2020 155* **2020**, *15* (5), 348−355.

(5) Gordeeva, L. G.; Tu, Y. D.; Pan, Q.; Palash, M. L.; Saha, B. B.; Aristov, Y. I.; Wang, R. Z. Metal-Organic Frameworks for Energy Conversion and Water Harvesting: A Bridge between Thermal Engineering and Material Science. *Nano Energy* **2021**, *84*, 105946.

(6) Xu, J.; Chao, J.; Li, T.; Yan, T.; Wu, S.; Wu, M.; Zhao, B.; Wang, R. Near-Zero-Energy Smart Battery Thermal Management Enabled by Sorption Energy Harvesting from Air. *ACS Cent. Sci.* **2020**, *6* (9), 1542−1554.

(7) Feng, C.; Yang, P.; Liu, H.; Mao, M.; Liu, Y.; Xue, T.; Fu, J.; Cheng, T.; Hu, X.; Fan, H. J.; Liu, K. Bilayer Porous Polymer for Efficient Passive Building Cooling. *Nano Energy* **2021**, *85*, 105971.

(8) Li, R.; Shi, Y.; Wu, M.; Hong, S.; Wang, P. Photovoltaic Panel Cooling by Atmospheric Water Sorption-Evaporation Cycle. *Nat. Sustain.* **2020**, *3* (8), 636−643.

(9) Wang, C.; Hua, L.; Yan, H.; Li, B.; Tu, Y.; Wang, R. A Thermal Management Strategy for Electronic Devices Based on Moisture Sorption-Desorption Processes. *Joule* **2020**, *4* (2), 435−447.

(10) Pu, S.; Liao, Y.; Chen, K.; Fu, J.; Zhang, S.; Ge, L.; Conta, G.; Bouzarif, S.; Cheng, T.; Hu, X.; Liu, K.; Chen, J. Thermogalvanic Hydrogel for Synchronous Evaporative Cooling and Low-Grade Heat Energy Harvesting. *Nano Lett.* **2020**, *20* (5), 3791−3797.

(11) Narayanan, S.; Kim, H.; Umans, A.; Yang, S.; Li, X.; Schiffres, S. N.; Rao, S. R.; McKay, I. S.; Wang, E. N.; Rios Perez, C. A.; Hidrovo, C. H. A Thermophysical Battery for Storage-Based Climate Control. *Appl. Energy* **2017**, *189*, 31−43.

(12) Narayanan, S.; Li, X.; Yang, S.; Kim, H.; Umans, A.; McKay, I. S.; Wang, E. N. Thermal Battery for Portable Climate Control. *Appl. Energy* **2015**, *149*, 104−116.

(13) Narayanan, S.; Yang, S.; Kim, H.; Wang, E. N. Optimization of Adsorption Processes for Climate Control and Thermal Energy Storage. *Int. J. Heat Mass Transfer* **2014**, *77*, 288−300.

(14) Zhao, F.; Zhou, X.; Liu, Y.; Shi, Y.; Dai, Y.; Yu, G. Super Moisture-Absorbent Gels for All-Weather Atmospheric Water Harvesting. *Adv. Mater.* **2019**, *31* (10), 1806446.

(15) Li, R.; Shi, Y.; Alsaedi, M.; Wu, M.; Shi, L.; Wang, P. Hybrid Hydrogel with High Water Vapor Harvesting Capacity for Deployable Solar-Driven Atmospheric Water Generator. *Environ. Sci. Technol.* **2018**, *52* (19), 11367−11377.

(16) Guo, Y.; Fang, Z.; Yu, G. Multifunctional Hydrogels for Sustainable Energy and Environment. *Polym. Int.* **2021**, *70* (10), 1425−1432.

(17) Yilmaz, G.; Meng, F. L.; Lu, W.; Abed, J.; Peh, C. K. N.; Gao, M.; Sargent, E. H.; Ho, G. W. Autonomous Atmospheric Water Seeping MOF Matrix. *Sci. Adv.* **2020**, *6* (42), No. eabc8605.

(18) Kallenberger, P. A.; Fröba, M. Water Harvesting from Air with a Hygroscopic Salt in a Hydrogel-Derived Matrix. *Commun. Chem.* **2018**, *1* (1), 1−6.

(19) Entezari, A.; Ejeian, M.; Wang, R. Super Atmospheric Water Harvesting Hydrogel with Alginate Chains Modified with Binary Salts. *ACS Mater. Lett.* **2020**, *2* (5), 471−477.

(20) Nandakumar, D. K.; Ravi, S. K.; Zhang, Y.; Guo, N.; Zhang, C.; Tan, S. C. A Super Hygroscopic Hydrogel for Harnessing Ambient Humidity for Energy Conservation and Harvesting †. *Energy Environ. Sci.* **2018**, *11*, 2179.

(21) Zhou, X.; Lu, H.; Zhao, F.; Yu, G. Atmospheric Water Harvesting: A Review of Material and Structural Designs. *ACS Mater. Lett.* **2020**, *2* (7), 671−684.

(22) Zhou, X.; Zhang, P.; Zhao, F.; Yu, G. Super Moisture Absorbent Gels for Sustainable Agriculture via Atmospheric Water Irrigation. *ACS Mater. Lett.* **2020**, *2* (11), 1419−1422.

(23) Gwadera, M.; Kupiec, K. Investigation of Water Vapour Adsorption on Silica Gel Grains Coated on a Metal Pipe. *Adsorpt. Sci. Technol.* **2015**, *33* (5), 499−511.

(24) Chua, H. T.; Ng, K. C.; Chakraborty, A.; Oo, N. M.; Othman, M. A. Adsorption Characteristics of Silica Gel + Water Systems. *J. Chem. Eng. Data* **2002**, *47* (5), 1177−1181.

(25) Ng, E. P.; Mintova, S. Nanoporous Materials with Enhanced Hydrophilicity and High Water Sorption Capacity. *Microporous Mesoporous Mater.* **2008**, *114* (1−3), 1−26.

(26) Castillo, J. M.; Silvestre-Albero, J.; Rodriguez-Reinoso, F.; Vlugt, T. J. H.; Calero, S. Water Adsorption in Hydrophilic Zeolites:

Experiment and Simulation. *Phys. Chem. Chem. Phys.* **2013**, *15* (40), 17374−17382.
(27) Simonot-Grange, M. H. Thermodynamic and Structural Features of Water Sorption in Zeolites. *Clays Clay Miner. 1979 276* **1979**, *27* (6), 423−428.
(28) Liu, X.; Wang, X.; Kapteijn, F. Water and Metal-Organic Frameworks: From Interaction toward Utilization. *Chem. Rev.* **2020**, *120* (16), 8303−8377.
(29) Canivet, J.; Fateeva, A.; Guo, Y.; Coasne, B.; Farrusseng, D. Water Adsorption in MOFs: Fundamentals and Applications. *Chem. Soc. Rev.* **2014**, *43* (16), 5594−5617.
(30) LaPotin, A.; Kim, H.; Rao, S. R.; Wang, E. N. Adsorption-Based Atmospheric Water Harvesting: Impact of Material and Component Properties on System-Level Performance. *Acc. Chem. Res.* **2019**, *52* (6), 1588−1597.
(31) Sircar, S.; Hufton, J. R. Why Does the Linear Driving Force Model for Adsorption Kinetics Work? *Adsorpt. 2000 62* **2000**, *6* (2), 137−147.
(32) Flory, P. J. *Principles of Polymer Chemistry*; Cornell University Press: Ithaca, NY, 1953.
(33) Yoon, J.; Cai, S.; Suo, Z.; Hayward, R. C. Poroelastic Swelling Kinetics of Thin Hydrogel Layers: Comparison of Theory and Experiment. *Soft Matter* **2010**, *6* (23), 6004−6012.
(34) Bertrand, T.; Peixinho, J.; Mukhopadhyay, S.; MacMinn, C. W. Dynamics of Swelling and Drying in a Spherical Gel. *Phys. Rev. Appl.* **2016**, *6* (6), 064010.
(35) Conde, M. R. Properties of Aqueous Solutions of Lithium and Calcium Chlorides: Formulations for Use in Air Conditioning Equipment Design. *Int. J. Therm. Sci.* **2004**, *43* (4), 367−382.
(36) Parker, V. *Thermal Properties of Aqueous Uni-Univalent Electrolytes*; U.S. Government Printing Office: Washington, DC, 1965; Vol. *2*.
(37) Blandamer, M. J. Structure and Properties of Aqueous Salt Solutions. *Q. Rev. Chem. Soc.* **1970**, *24* (2), 169−184.
(38) Long, F. A.; McDevit, W. F. Activity Coefficients of Nonelectrolyte Solutes in Aqueous Salt Solutions. *Chem. Rev.* **1952**, *51* (1), 119−169.
(39) Atkins, P.; de Paula, J. *Atkins' Physical Chemistry*; W. H. Freeman and Company: New York, 2006.
(40) Mills, A. F. *Heat and Mass Transfer*; McGraw-Hill: New York, 1994.
(41) MARSHALL, T. J. THE DIFFUSION OF GASES THROUGH POROUS MEDIA. *J. Soil Sci.* **1959**, *10* (1), 79−82.
(42) Tartakovsky, D. M.; Dentz, M. Diffusion in Porous Media: Phenomena and Mechanisms. *Transp. Porous Media* **2019**, *130* (1), 105−127.
(43) Biot, M. A. General Theory of Three-Dimensional Consolidation. *J. Appl. Phys.* **1941**, *12* (2), 155−164.
(44) Hui, C. Y.; Muralidharan, V. Gel Mechanics: A Comparison of the Theories of Biot and Tanaka, Hocker, and Benedek. *J. Chem. Phys.* **2005**, *123* (15), 154905.
(45) Tokita, M.; Tanaka, T. Friction Coefficient of Polymer Networks of Gels. *J. Chem. Phys.* **1991**, *95* (6), 4613−4619.
(46) Limousin, G.; Gaudet, J. P.; Charlet, L.; Szenknect, S.; Barthès, V.; Krimissa, M. Sorption Isotherms: A Review on Physical Bases, Modeling and Measurement. *Appl. Geochem.* **2007**, *22* (2), 249−275.
(47) Reuge, N.; Fede, P.; Berthoumieu, J.-F.; Foucoin, F.; Simonin, O. Modeling of the Denebulization of Warm Fogs by Hygroscopic Seeding: Effect of Various Operating Conditions and of the Turbulence Intensity. *J. Appl. Meteorol. Climatol.* **2017**, *56* (2), 249−261.
(48) Ponomarenko, I. V.; Glaznev, I. S.; Gubar, A. V.; Aristov, Y. I.; Kirik, S. D. Synthesis and Water Sorption Properties of a New Composite "CaCl2 Confined into SBA-15 Pores. *Microporous Mesoporous Mater.* **2010**, *129* (1-2), 243−250.
(49) Ally, M. R. Solute and Solvent Activities of CaCl2(Aq) Solutions from the Adsorption Isotherm Treatment. *J. Chem. Eng. Data* **1999**, *44* (4), 792−797.
(50) Wang, Q.; Zhao, L.; Li, C.; Cao, Z. The Decisive Role of Free Water in Determining Homogenous Ice Nucleation Behavior of Aqueous Solutions. *Sci. Reports 2016 61* **2016**, *6* (1), 1−8.
(51) Louf, J. F.; Datta, S. S. Poroelastic Shape Relaxation of Hydrogel Particles. *Soft Matter* **2021**, *17* (14), 3840−3847.
(52) Cuccia, N. L.; Pothineni, S.; Wu, B.; Mendez Harper, J.; Burton, J. C. Pore-Size Dependence and Slow Relaxation of Hydrogel Friction on Smooth Surfaces. *Proc. Natl. Acad. Sci. U. S. A.* **2020**, *117* (21), 11247−11256.
(53) Stellwagen, N. C. Apparent Pore Size of Polyacrylamide Gels: Comparison of Gels Cast and Run in Tris-Acetate-EDTA and Tris-Borate-EDTA Buffers. *Electrophoresis* **1998**, *19* (10), 1542−1547.
(54) Hua, J.; Ng, P. F.; Fei, B. High-Strength Hydrogels: Microstructure Design, Characterization and Applications. *J. Polym. Sci., Part B: Polym. Phys.* **2018**, *56* (19), 1325−1335.

https://doi.org/10.1021/acs.nanolett.1c04216
Nano Lett. XXXX, XXX, XXX−XXX